

Article

A Novel Exoskeleton Design and Numerical Characterization for Human Gait Assistance

Cristian Copilusi ^{1,*} , Marco Ceccarelli ² , Sorin Dumitru ¹, Ionut Geonea ¹ , Alexandru Margine ¹ and Dorin Popescu ³

¹ Applied Mechanics and Civil Engineering Department, Faculty of Mechanics, University of Craiova, 200512 Craiova, Romania; sorin.dumitru@edu.ucv.ro (S.D.); ionut.geonea@edu.ucv.ro (I.G.); alexandru.margine@edu.ucv.ro (A.M.)

² Applied Mechanics Department, University of Rome Tor Vergata, 00133 Rome, Italy; marco.ceccarelli@uniroma2.it

³ Automation, Electronics and Mechatronics Department, Faculty of Automation, Computers and Electronics, University of Craiova, 200440 Craiova, Romania; dorin.popescu@edu.ucv.ro

* Correspondence: cristian.copilusi@edu.ucv.ro; Tel.: +40-747222771

Abstract: This paper addressed attention to the design of a new lower limb exoskeleton that can be used for human gait assistance as based on kinematic considerations. The designed leg exoskeleton had on its own structure a combination of three mechanism types, namely a Chebyshev mechanism, a pantograph, and a Stephenson six-bar mechanism. The design core focused on inserting the Stephenson six-bar mechanism in order to obtain an imposed motion at the ankle joint level. Numerical simulations of the designed lower limb exoskeleton have been developed and the obtained results demonstrate the engineering feasibility of the proposed prototype, with a characterization of satisfactory operation performance.

Keywords: exoskeletons; walking assistance; mechanism design; simulation; six-bar mechanism; kinematics



Citation: Copilusi, C.; Ceccarelli, M.; Dumitru, S.; Geonea, I.; Margine, A.; Popescu, D. A Novel Exoskeleton Design and Numerical Characterization for Human Gait Assistance. *Machines* **2023**, *11*, 925. <https://doi.org/10.3390/machines11100925>

Academic Editor: Dan Zhang

Received: 17 August 2023

Revised: 19 September 2023

Accepted: 21 September 2023

Published: 26 September 2023



Copyright: © 2023 by the authors. Licensee MDPI, Basel, Switzerland. This article is an open access article distributed under the terms and conditions of the Creative Commons Attribution (CC BY) license (<https://creativecommons.org/licenses/by/4.0/>).

1. Introduction

Today, a variety of rehabilitation systems can be found, as dedicated to human gait assistance, from simple solutions to complex ones. Most of them are especially designed for using in gait rehabilitation processes or assistance in case of adult persons. A few of them are dedicated to children with locomotion system problems.

In the case of children, it is well known that these are in a continuous growth and after some small time periods, these rehabilitation systems need to be reconfigured. In their cases, a few pathology cases can be found like congenital malformations, brittle bone disease, or neurological problems. For most of the cases in children, it is necessary to use special therapy in order to give them the ability to walk.

Thus, in recent decades, physicians developed collaborations for inserting and using modern systems for human gait assistance. In this category, exoskeletons especially designed to help children with special needs to walk again can be found.

Most of the existent exoskeleton solutions are complex ones [1–9], but they can also be purchased at high prices. In addition, they have sensors, a large number of actuators controlled through electronic devices such as computer processors, making the device bulky and uncomfortable.

Those rehabilitation systems, which use an exoskeleton, use linear or rotational actuators placed directly on the desired joint and for command and control, there are sensors placed at the muscle group level in order to acquire signals transmitted to a sensor unit for motion correlations during human gait phases.

Generally referring to low-cost solutions, these often do not accomplish specific needs for walking activity, due to the fact that they cannot replicate a natural motion for all

main locomotion system joints (hip, knee, and ankle joints)—e.g., [10]. In this category, exoskeletons characterized by a single DoF linkage-based mechanisms can be found. These exoskeletons have a simple and fair structure, are lightweight, and these can replicate human gait patterns in the sagittal plane [11]. Due to a single DoF, a suitable actuator can be used in their structure, and this can lower the price and simplify the control architecture.

Referring to these exoskeleton types, the targeted joints for developing the desired motions can be assured through mechanism linkages, and these can be found in several configurations like four-bar [11], six-bar [12,13], seven-bar [14], eight-bar [15,16], and ten-bar [17] mechanisms for the purpose of hip, knee, and ankle joints trajectory generation.

In a previous work [17], a leg exoskeleton solution was developed that combines two mechanisms, namely Chebyshev and a pantograph for actuating only the hip and knee joints. This can fulfill a partial motion of the human locomotion systems due to the fact that the ankle joint was neglected.

In [18], the design was extended by inserting a cam mechanism in the leg exoskeleton structure in order to have a fully actuated system. After choosing this solution, in the end, major disadvantages occur and these were represented by wear, imprecise motions during overloads, a backlash between the cam follower and cam body, and these can lead to improper ankle joint motions during human gait phases.

The contribution herein is in the form of implementing a six-bar mechanism, namely the Stephenson II type mechanism, that can replace the cam mechanism from the previous solution [18] and can accomplish the desired foot trajectory during human walking activity with respect to human motion laws developed for hip, knee, and ankle joints. The Stephenson II mechanism was also applied for designing exoskeletons in [19,20] with fully actuated joints by combining this mechanism type.

For validating the proposed solution, it can be performed an inverse or a direct kinematic analysis, dynamic analyses, and furthermore numerical simulations. Thus, the work core will be focused on a direct kinematic analysis and certify it through numerical simulations carried out on a parametrized model with MSC Adams software version R17 aid.

The paper is organized as follows: Section 2 represents an experimental analysis of a human gait in a particular case (four years old child) for obtaining hip, knee, and ankle joint motion laws and foot trajectory. Section 3 focused on a structural analysis of the proposed linkage mechanism, which will be necessary to obtain further kinematic schemes of the leg exoskeleton solution. Section 4 presents a kinematic analysis that provides for numerical simulations of a parametrized model. A simplified CAD model elaborated for numerical simulations under the MSC Adams environment and numerical results are presented and discussed in Section 5. Final conclusions of the proposed research are drawn and provided in the last section of this paper.

2. Experimental Analysis of a Child Gait

For the experimental analysis of walking activity, a four-year-old healthy child was chosen and the aim of this was to determine the hip, knee, and ankle joints motion laws and foot trajectory during a complete gait. For this analysis, a piece of equipment called CONTEMPLAS [21] was used and the working principle of it was to track some specific markers attached to the human lower limb. These markers are reflective ones, and the software TEMPLO Motion 2016, associated with this equipment, has the ability to target and track these markers. The markers position was accomplished at the recommendations of a physician in order to identify each joint center position. The markers displacement can be seen in Figure 1. According to Figure 1, a set of 10 markers can be remarked and also a global coordinate reference system positioned on the treadmill frame. This position was also specified during equipment calibration to establish the correct values of the desired results.

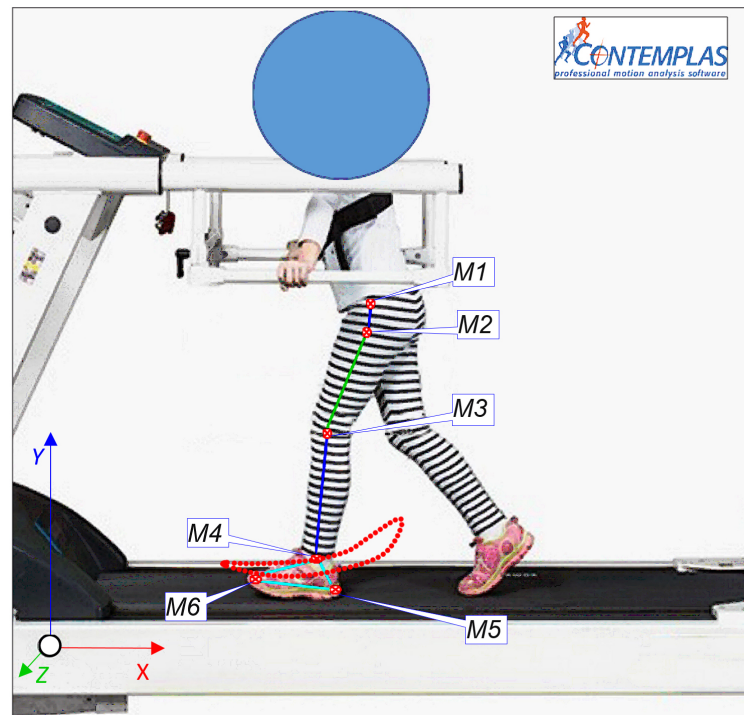


Figure 1. Snapshot during an experimental test of the proposed human subject.

In Figure 1, the following notations can be identified: M1—pelvis mass center location; M2—hip joint; M3—knee joint; M4—ankle joint; M5—heel extreme point; M6—distal phalanges extreme point.

During a complete gait analysis, the child developed, at the level of the foot, a trajectory which is valuable for this research during experimental evaluation. This will be considered as a reference point for the desired trajectory of the designed leg exoskeleton. Also, this can be observed in Figure 1. Two high-speed cameras with a speed of 350 frames/s recorded the human locomotion system motions. Both cameras were placed on the lateral side of the child in order to record each limb's motion for a complete gait. Thus, the results developed by the left lower limb will be used for this experimental research. The interesting results are shown in Figures 2–5.

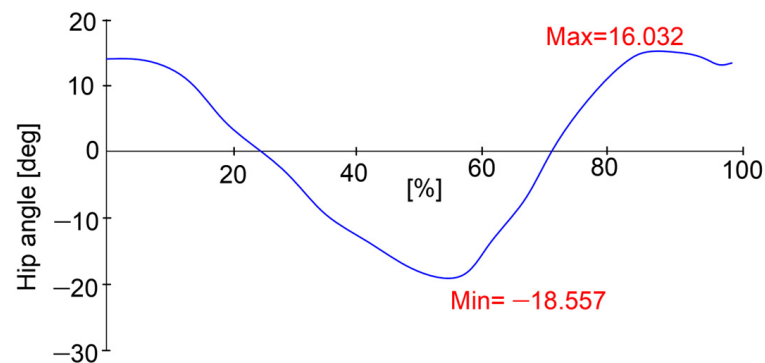


Figure 2. Hip motion law [degrees] for a complete gait [100%].

All experimental results were compared with the existing ones in the specific literature data, according to [22], and the evaluated lower limb was the left one. By having in sight the reported plot from Figure 2, it can be observed that the maximum value of the hip joint during a complete gait reached a maximum value of 16.03 degrees and a minimum value of -18.5 degrees. This means that the analyzed joint developed an angular amplitude of 34.5 degrees.

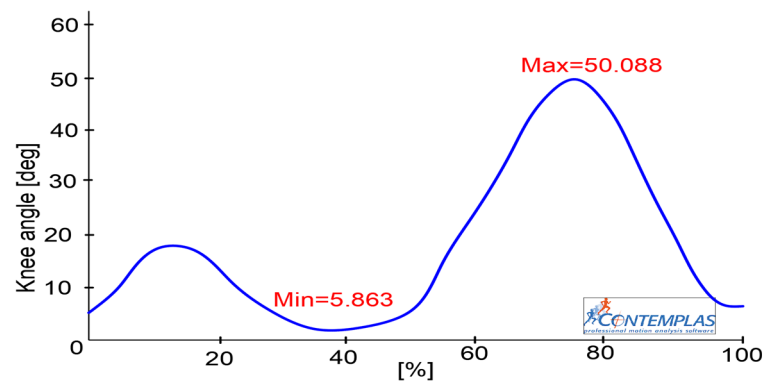


Figure 3. Acquired data of knee motion [degrees] for a complete gait [100%].

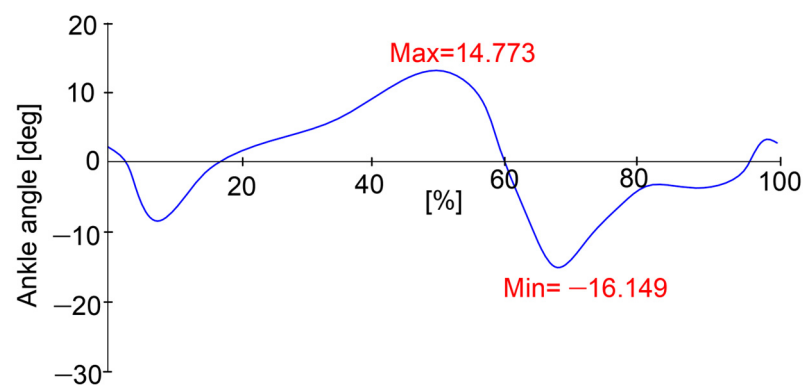


Figure 4. Acquired data of ankle motion [degrees] for a complete gait [100%].

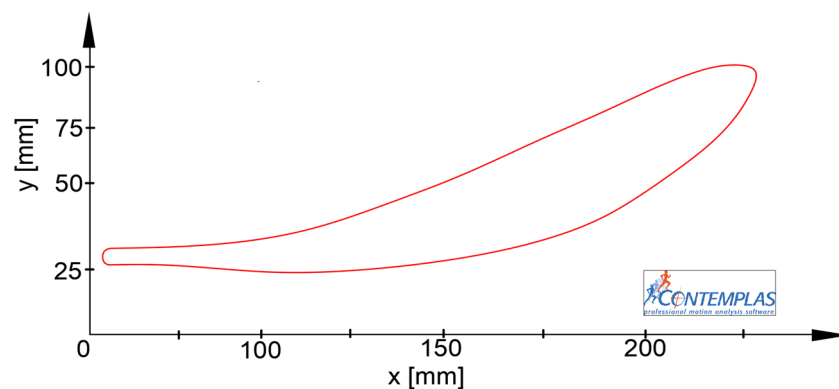


Figure 5. Foot trajectory (M6—point) recorded for a complete gait of the proposed human subject.

In the case of the knee joint, the obtained results are reported in the graph from Figure 3. In the reported graph, it can be remarked that the maximum value of the knee joint flexion was equal to 50.08 degrees and a minimum one equal to 5.8 degrees. Thus, it resulted in an angular amplitude of the knee joint flexion equal to 44.2 degrees.

Simultaneously, the ankle joint was also analyzed and for dorsal/plantar flexions, a maximum value of 14.7 degrees, respectively, and a minimum one equal to -16.1 degrees, according to the reported plot in Figure 4, were recorded. This means an angular amplitude equal to 30.9 degrees.

An essential experimental result was related to the M6—point foot trajectory, which is presented in Figure 5. From this graph, the curve and the maximum and minimum values on x-y coordinates can be considered, in order to validate the proposed lower limb exoskeleton.

Furthermore, the experimental analysis gave the opportunity to evaluate the anthropometric data of the proposed human subject. Thus, the lower limb segment length was recorded, which will be used as input data for parametrizing the lower limb exoskeleton's main dimensions. These dimensional parameters were $L_{\text{femur}} = 315 \text{ mm}$; $L_{\text{tibia}} = 292 \text{ mm}$; $L_{\text{foot}} = 122 \text{ mm}$.

For the proposed work, the motion laws variation reported in Figures 2–4 will be represented by angles with the notations from Figure 6.

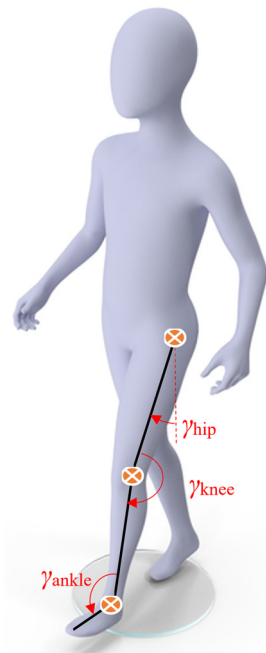


Figure 6. Angles identification for the corresponding motion laws in Figures 2–4.

3. Conceptual Design of the Lower Limb Exoskeleton Mechanism

The design for a novel leg exoskeleton concept starts from previous solutions, namely a Chebyshev, pantograph, and cam mechanisms combination. The aim was to adapt a Stephenson III six-bar mechanism for ankle joint actuation extension. The reason for adapting this mechanism is given by the fact that this mechanism is an optimum solution that can assure lower limb trajectories required for gait rehabilitation purposes, as pointed out in [19]. The mentioned mechanisms are represented in Figure 7.

Some structural parameters of the solutions shown in Figure 7 are listed in Table 1, which are characterized by the mobility range.

Table 1. Mechanism structural comparison based on Figure 7.

Mechanism	Number of Links	Number of Joints	DoF	Mobility Range
Figure 7a	5	7 revolute joints	1DoF = 7	1
Figure 7b	6	8 revolute joints	1DoF = 8	1
Figure 7c	5	7 revolute joints	2DoF = 1 (cam mechanism) 1DoF = 7	1

Thus, the cam mechanism adapted for a leg exoskeleton design, Figure 7b, gave a fair solution for elaborating a prototype, as reported in [23]. The obtained leg exoskeleton solution from Figure 7b was characterized by the cam-mechanism actuation for ankle joint motion and it had some disadvantages, like imprecise motions during overloads, a backlash between the cam follower and the cam body, and wear. This affected the gait phases through improper motions.

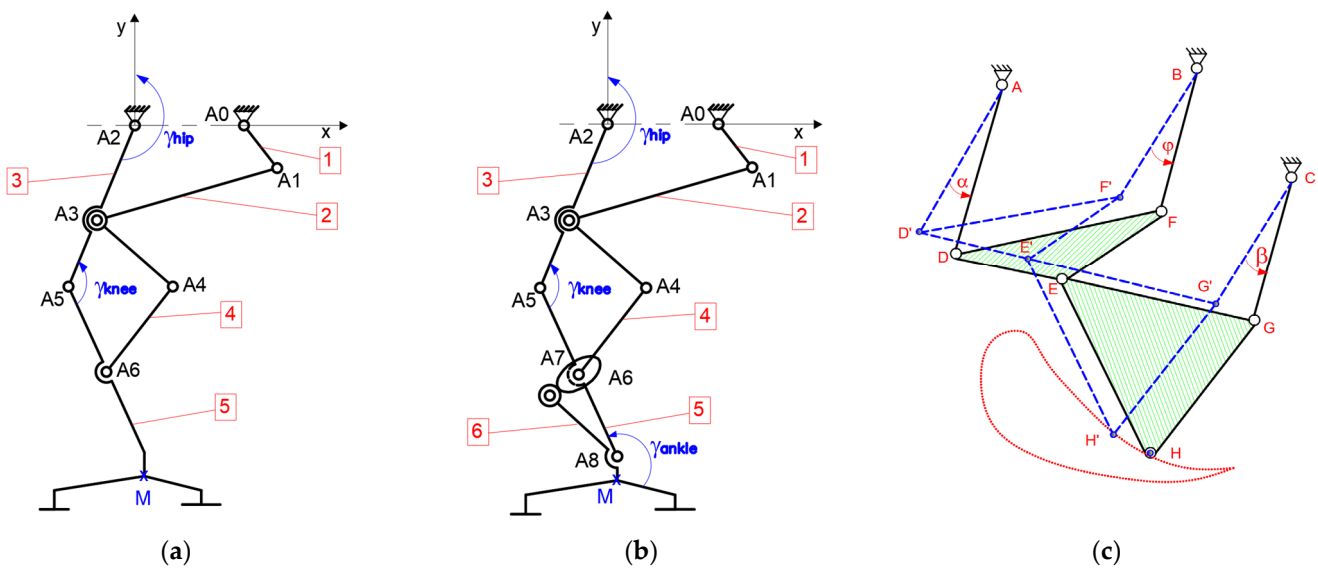


Figure 7. Mechanisms for a new lower limb exoskeleton: (a)—Chebyshev and pantograph mechanism [18]; (b)—Chebyshev, pantograph, and cam mechanism [23]; (c)—Stephenson III six-bar mechanism [23].

By considering the existent structural scheme from Figure 7a and the general scheme of Stephenson III six-bar mechanism, from Figure 7c, a new elaborated lower limb exoskeleton concept can be considered. From this, a structural scheme only to actuate the ankle joint, and to have a proper trajectory similar to the one reported in Figure 5, was obtained. This adapted mechanism is shown through a structural scheme from Figure 8.

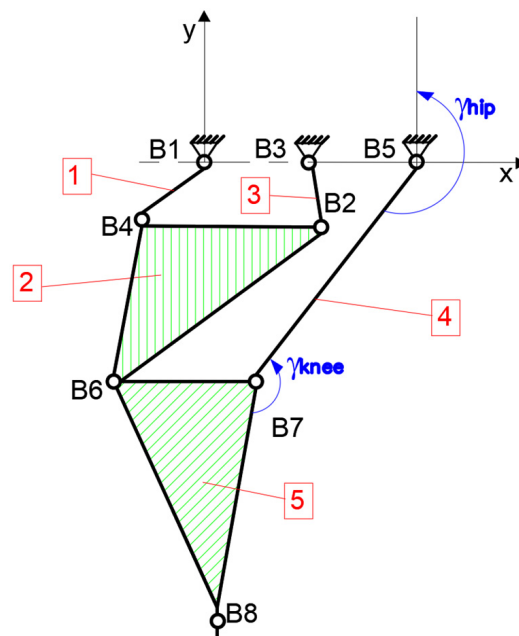


Figure 8. Stephenson III six-bar mechanism adapted for ankle actuation joint.

The proposed solution combined the structural scheme of Stephenson III six-bar mechanism from Figure 8 with the one presented in Figure 7a. Thus, there will be two main parallel mechanisms, one for actuating hip and knee joints composed from Chebyshev and a pantograph mechanism combination, and the other only for actuating the ankle joint, namely Stephenson III six-bar mechanism, as can be seen in Figure 9.

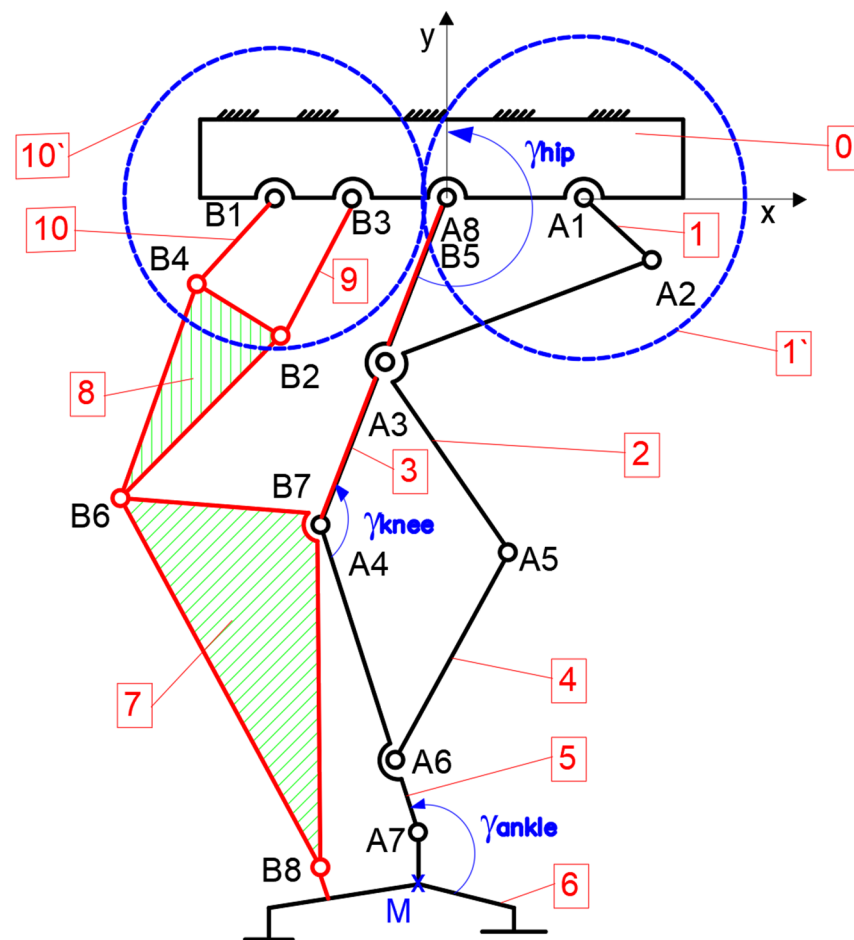


Figure 9. Conceptual scheme of new lower limb exoskeleton.

From Figure 9, it can be remarked that the drive link is no. 1 for actuating hip and knee joints under dictating angles γ_{hip} and γ_{knee} . Therefore, for the Stephenson III six-bar mechanism, the drive link was no. 1 according to the scheme from Figure 8, but in the case of this parallel mechanism, the drive link will be substituted through the link no. 9 and will receive motion from a pair of gears, respectively, $10'$ and $1'$ with 1:1 ratio.

The mechanism functionality, based on the scheme in Figure 9, was the following. The drive link 1 was fixed with the gear 1 and rotated through revolute joint A1 in accordance with the fixed frame 0. This actuated the Chebyshev mechanism through links no. 2 and 3 and the revolute joints A2, A8, and A3. In this way, link no. 3 equivalent to the femur will rotate with the angle γ_{hip} and the A8 revolute joint equivalent to the exoskeleton hip. On the other hand, the link no. 2 architecture is characterized by an angle of 90 degrees, which allows actuating the pantograph linkage made from links no. 2, 4, and 5, respectively, revolute joints A3, A4, A5, and A6. Thus, link no. 5 is equivalent to the tibia segment and it connects to link no. 3 through revolute joint A4, which is equivalent to the knee joint and this rotates with the angle γ_{knee} . For actuating the ankle joint, the Stephenson III six-bar mechanism placed in parallel with the other one will be used. For this, the motion is received from gear no. $10'$ which is fixed with link no. 10. This link will actuate the first part of the mechanism linkage through the revolute joints B1, B4, B2, B3, and B6. The revolute joint B6 is common with the second part of the linkage, namely links no. 7, 6, and 3. This part is characterized by the revolute joints B6, B7, B8, and B5. One remark is that link no. 3 is common for both mechanism linkages and corresponds to the femur segment. Link no. 7 will actuate with a proper motion angle γ_{ankle} the revolute joint A7, and link no. 6, respectively, point M will describe an imposed trajectory as the one reported in Figure 5.

Thus, the mobility range is equal to one due to 10 links, 28 revolute joints, and a pair of gears. The entire linkage from Figure 9 will be considered as a starting point for further kinematic and dynamic analyses.

4. Kinematic Analysis

For the kinematic analysis of the novel lower limb exoskeleton, a kinematic scheme was elaborated, in accordance with the structural scheme presented in Figure 9, as can be seen in Figure 10.

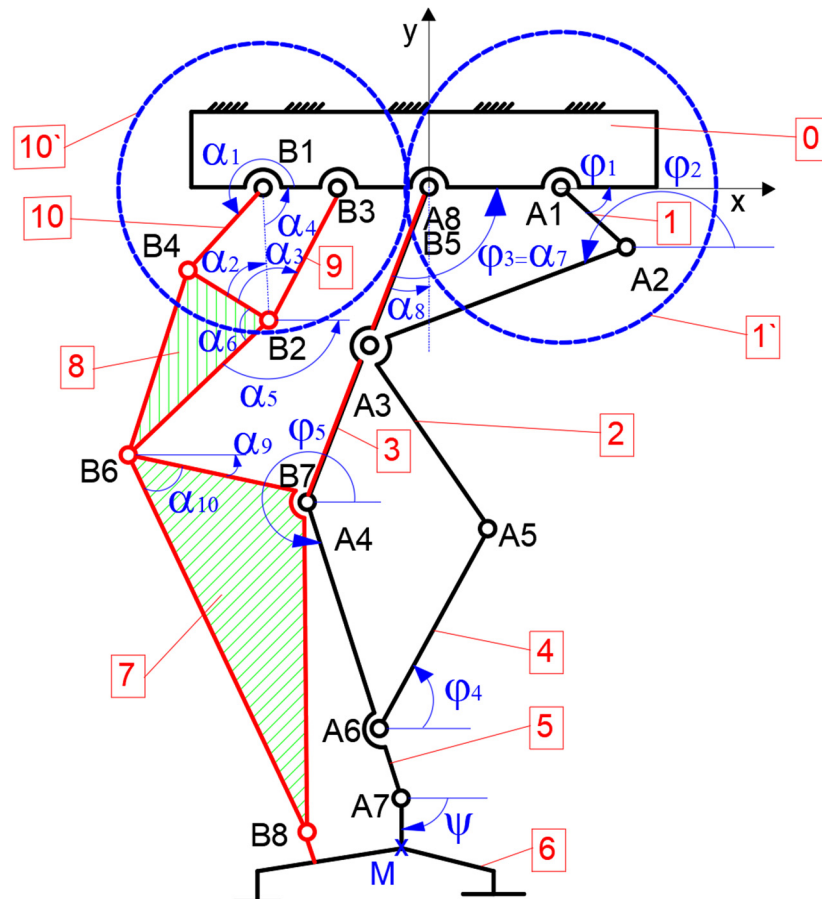


Figure 10. Human lower limb exoskeleton kinematic model.

The aim of this analysis was to determine the angular positions of the target equivalent joints, namely hip, knee, and ankle. Another objective was to obtain a proper M-point trajectory, similar to the one presented in Figure 5.

The mathematical model elaborated in this section was a parametrized one, which allowed us to adjust the proper main dimensions similar to the ones of the child used in the experimental analyses frame.

From Figure 10, two parallel mechanisms can be observed, namely an adapted Stephenson III six-bar mechanism for ankle joint actuation, and another one composed of a Chebyshev and a pantograph linkages for actuating hip and knee joints.

4.1. Chebyshev and Pantograph Mechanism Kinematic Analysis

The kinematic model of the proposed mechanism is shown in Figure 11, and the obtained equations will demonstrate the performance and operations for hip and knee joints.

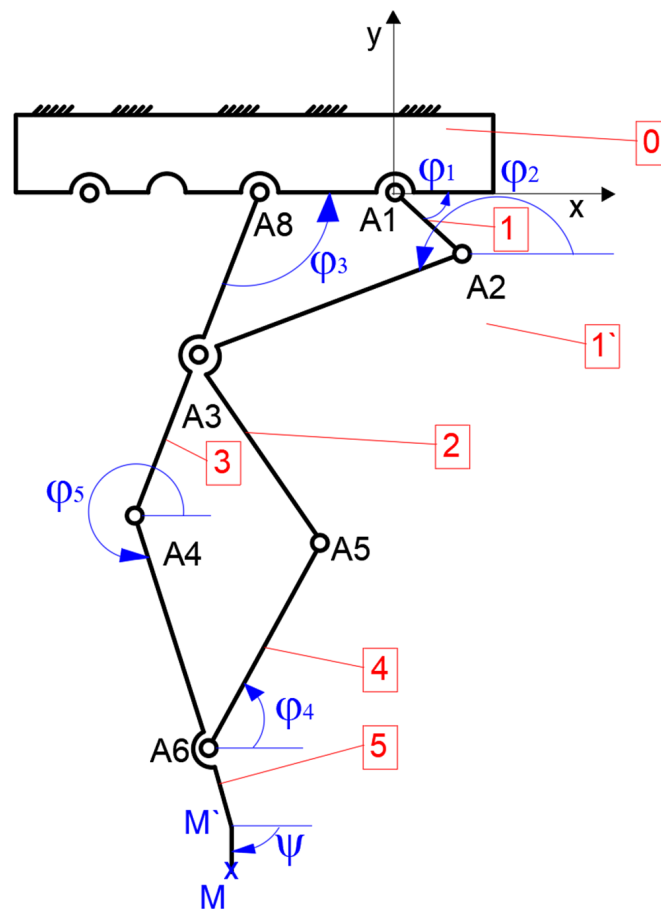


Figure 11. A kinematic model for actuating hip and knee joints.

From Figure 11, the local coordinate system is located in the A1 revolute joint. The following convention of the angle notation holds: $\varphi_3 = \gamma_{\text{hip}}$ and $\varphi_5 = \gamma_{\text{knee}}$.

The point A4 position can be calculated as a function of the drive link angle φ_1 , in accordance with the XOY reference system, and the kinematic parameters of the Chebyshev linkage O, A2, A8, and A3.

Thus, the position of point A3 can be evaluated in accordance with the local coordinate system by

$$\begin{aligned} x_{A3} &= x_{A8} + l_{A3A8} \cos \varphi_3 \\ y_{A3} &= y_{A8} - l_{A3A8} \sin \varphi_3 \end{aligned} \tag{1}$$

The position of M' -point, according with the base frame 0 can be given as

$$\begin{aligned} x_{M'} &= x_{A4} + l_{A4M'} \cos \varphi_5 \\ y_{M'} &= y_{A4} + l_{A4M'} \sin \varphi_5 \end{aligned} \tag{2}$$

In this way, point M position can be calculated by

$$\begin{aligned} x_M &= x_{M'} + l_{MM'} \cos \psi \\ y_M &= y_{M'} + l_{MM'} \sin \psi \end{aligned} \tag{3}$$

If it needs to evaluate velocities for points A8, M' , and M , Equations (1)–(3) and the angles φ_i (with $i = 1$ to 5) can be solved by considering the closure loops equations as a function of $\varphi_1 = \omega \cdot t$ to give

$$\varphi_2 = 2 \tan^{-1} \left(\frac{\Delta_1 \pm \sqrt{\Delta_1^2 + \Delta_2^2 - \Delta_3^2}}{\Delta_2 - \Delta_3} \right) \tag{4}$$

$$\varphi_3 = 2 \tan^{-1} \left(\frac{\Delta_4 \pm \sqrt{\Delta_4^2 + \Delta_5^2 - \Delta_6^2}}{\Delta_5 - \Delta_6} \right) \quad (5)$$

$$\varphi_4 = 2 \tan^{-1} \left(\frac{\Delta_7 \pm \sqrt{\Delta_7^2 + \Delta_8^2 - \Delta_9^2}}{\Delta_8 - \Delta_9} \right) \quad (6)$$

$$\varphi_5 = 2 \tan^{-1} \left(\frac{\Delta_{10} \pm \sqrt{\Delta_{10}^2 + \Delta_{11}^2 - \Delta_{12}^2}}{\Delta_{11} - \Delta_{12}} \right) \quad (7)$$

where:

$$\begin{aligned} \Delta_1 &= -2l_{A2A3}(y_{A2} - y_{A8}) \\ \Delta_2 &= -2l_{A2A3}(x_{A2} - x_{A8}) \\ \Delta_3 &= -(y_{A2} - y_{A8})^2 - (x_{A2} - x_{A8})^2 - l_{A2A3}^2 + l_{A3A8}^2 \\ \Delta_4 &= 2l_{A3A8}(y_{A2} - y_{A8}) \\ \Delta_5 &= 2l_{A3A8}(x_{A2} - x_{A8}) \\ \Delta_6 &= -(y_{A2} - y_{A8})^2 - (x_{A2} - x_{A8})^2 + l_{A2A3}^2 - l_{A3A8}^2 \\ \Delta_7 &= -2l_{A5A6}(y_{A4} - y_{A5}) \\ \Delta_8 &= -2l_{A5A6}(x_{A4} - x_{A5}) \\ \Delta_9 &= -(y_{A4} - y_{A5})^2 - (x_{A4} - x_{A5})^2 - l_{A5A6}^2 + l_{A4A6}^2 \\ \Delta_{10} &= -2l_{A4A6}(y_{A4} - y_{A5}) \\ \Delta_{11} &= -2l_{A5A6}(x_{A4} - x_{A5}) \\ \Delta_{12} &= -(y_{A4} - y_{A5})^2 - (x_{A4} - x_{A5})^2 + l_{A5A6}^2 - l_{A4A6}^2 \end{aligned} \quad (8)$$

The M-point acceleration can be obtained the following mathematical expressions

$$\begin{aligned} \ddot{x}_M &= -l_{A2A3} \left(\cos \varphi_2 \cdot \dot{\varphi}_2^2 + \sin \varphi_2 \cdot \ddot{\varphi}_2 \right) - l_{A3A4} \left(\cos \varphi_3 \cdot \dot{\varphi}_3^2 + \sin \varphi_3 \cdot \ddot{\varphi}_3 \right) - \\ &- l_{A4M'} \left(\cos \varphi_5 \cdot \dot{\varphi}_5^2 + \sin \varphi_5 \cdot \ddot{\varphi}_5 \right) \\ \ddot{y}_M &= l_{A4M'} \left(2 \cos \left(\ddot{\varphi}_5 + \dot{\varphi}_5^2 \right) - \sin \varphi_5 \cdot \dot{\varphi}_5^2 \right) \end{aligned} \quad (9)$$

4.2. Stephenson III Six-Bar

According to the kinematic scheme in Figure 10, the second mechanism linkage which actuates the ankle joint is shown separately, in Figure 12. A similar research was developed in [19].

From Figure 12, it can be seen that B1 was located at the level of the local coordinate system origin, B3 and B5 were revolute joints under the base frame.

Thus, the joints B5, B7, and B8 matched to the hip, knee, and ankle joints. This kinematic model had one actuator, namely the drive link no. 1 which will receive motion through a pair of gears namely 1 and 9'.

By calling at analytical geometry, it is necessary to differentiate each joint position based on the assumed angles (α_k with $k = 2$ to 10) in accordance with the input angle α_1 .

These angles and the distances between the revolute joints can be differentiated and represented by Equations (10)–(15).

$$\alpha_5 = \tan^{-1} \left(\frac{B_{4y} - B_{2y}}{B_{2x} - B_{4y}} \right) \quad (10)$$

$$\alpha_6 = \cos^{-1} \left(\frac{l_{B2B7}^2 + l_{B2B4}^2 - l_{B4B7}^2}{2 \cdot l_{B2B7} \cdot l_{B2B4}} \right) \quad (11)$$

$$\alpha_7 = \tan^{-1} \left(\frac{B_{7y} - B_{5y}}{B_{5x} - B_{7x}} \right) \tag{12}$$

$$\alpha_8 = \cos^{-1} \left(\frac{l_{B_5B_6}^2 + l_{B_5B_7}^2 - l_{B_6B_7}^2}{2 \cdot l_{B_5B_6} \cdot l_{B_5B_7}} \right) \tag{13}$$

$$\alpha_9 = \tan^{-1} \left(\frac{B_{6y} - B_{7y}}{B_{6x} - B_{7x}} \right) \tag{14}$$

$$\alpha_{10} = \cos^{-1} \left(\frac{l_{B_6B_7}^2 + l_{B_6B_8}^2 - l_{B_7B_8}^2}{2 \cdot l_{B_6B_7} \cdot l_{B_6B_8}} \right) \tag{15}$$

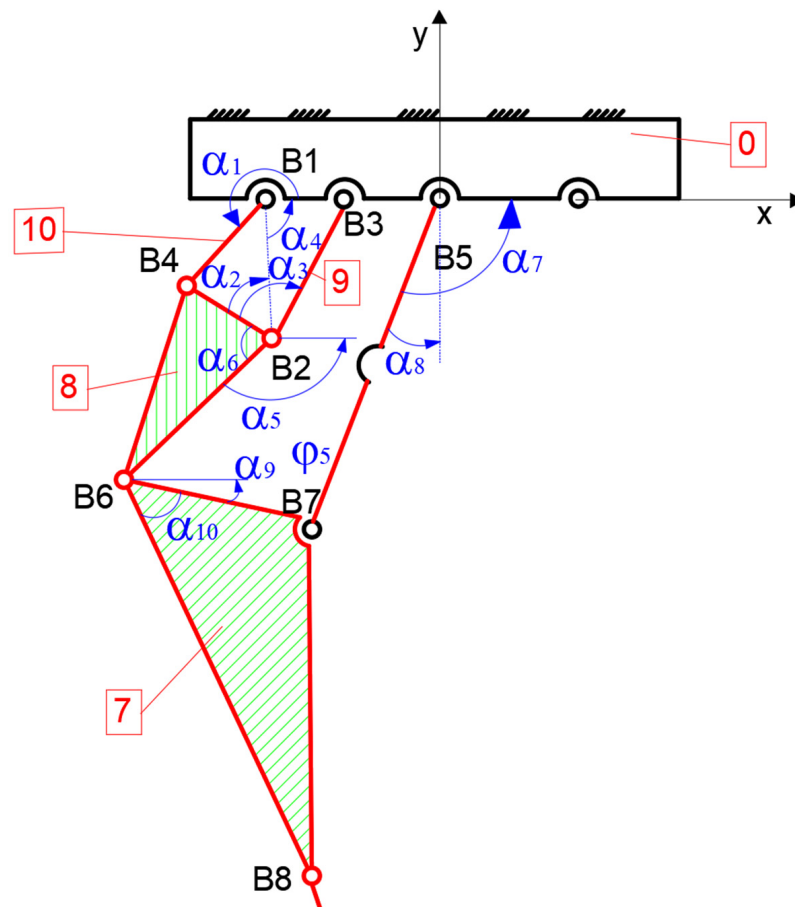


Figure 12. A kinematic model of the mechanism for actuating the ankle joint.

Thus, the positions of the mechanism characteristic points in accordance with the drive link angle α_1 can be computed by

$$\begin{cases} B_{4x} = B_{1x} + l_{B_1B_4} \cdot \cos \alpha_1 \\ B_{4y} = B_{1y} + l_{B_1B_4} \cdot \sin \alpha_1 \end{cases} \tag{16}$$

$$\begin{cases} B_{2x} = B_{3x} + l_{B_2B_3} \cdot \cos(\alpha_2 + \alpha_3 - \alpha_4) \\ B_{2y} = B_{3y} + l_{B_2B_3} \cdot \sin(\alpha_2 + \alpha_3 - \alpha_4) \end{cases} \tag{17}$$

$$\begin{cases} B_{7x} = B_{2x} + l_{B_2B_7} \cdot \cos(\alpha_5 + \alpha_6) \\ B_{7y} = B_{2y} - l_{B_2B_7} \cdot \sin(\alpha_5 + \alpha_6) \end{cases} \tag{18}$$

$$\begin{cases} B_{6x} = B_{5x} + l_{B5B6} \cdot \cos(\alpha_7 + \alpha_8) \\ B_{6y} = B_{5y} - l_{B5B6} \cdot \sin(\alpha_7 + \alpha_8) \end{cases} \quad (19)$$

$$\begin{cases} B_{8x} = B_{6x} + l_{B6B8} \cdot \cos(-\alpha_9 + \alpha_{10}) \\ B_{8y} = B_{6y} - l_{B6B8} \cdot \sin(-\alpha_9 + \alpha_{10}) \end{cases} \quad (20)$$

To compute velocities or accelerations, these can be obtained from successive differentials of Equations (16)–(20).

4.3. Numerical Processing

A kinematic analysis can be carried out by creating an algorithm under MAPLE software R12 environment for computing the kinematic models, which were previously presented. For this, it is necessary to have the length links of the mechanism presented in Figure 10 in numerical form. These values were obtained by taking into account the anthropometric data of the child, considered as reference positions.

Thus, for the first mechanism linkage, the following input data were considered: $l_{A1A2} = 25$ mm; $l_{A2A3} = 222.5$ mm; $l_{A4A8} = 305$ mm; $l_{A3A5} = 225$ mm; $l_{A5A6} = 240$ mm; $l_{A4M} = 292$ mm.

For the second mechanism, the input data are $l_{B1B4} = 25$ mm; $l_{B2B3} = 65$ mm; $l_{B4B2} = 85$ mm; $l_{B2B6} = 112.65$ mm; $l_{B5B7} = 305$ mm; $l_{B6B7} = 15.6$ mm; $l_{B6B8} = 243.54$ mm; $l_{B7B8} = 323.5$ mm, $l_{B4B6} = 115.15$ mm.

Thus, by processing the input data, numerical results have been obtained without considering the lower limb exoskeleton touching the ground. The targeted results are characterized by the angular positions of the hip, knee, and ankle joints. Also, the M-point trajectory under the x-y coordinate system represents an important result of performance characterization. These results are represented through the diagrams in Figures 13–17.

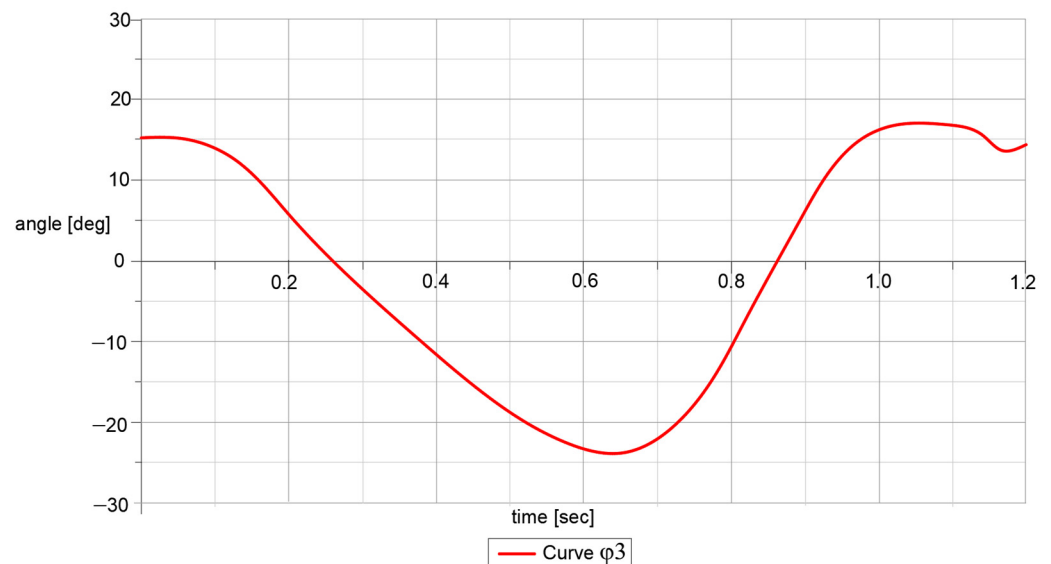


Figure 13. Computed hip motion law represented by the angle φ_3 [degrees] for a complete gait cycle [seconds].

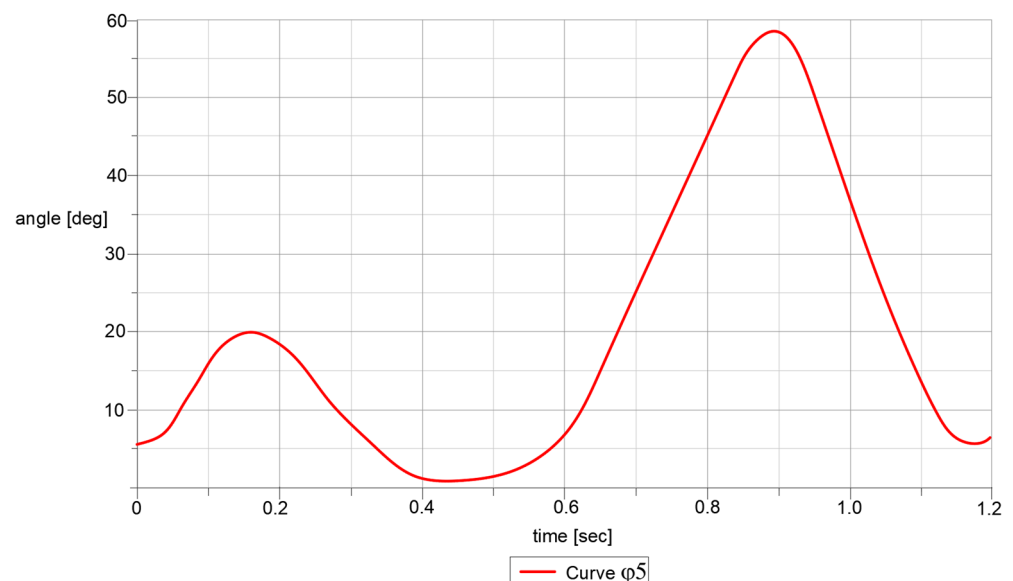


Figure 14. Computed knee motion law represented by the angle φ_5 [degrees] for a complete gait cycle [seconds].

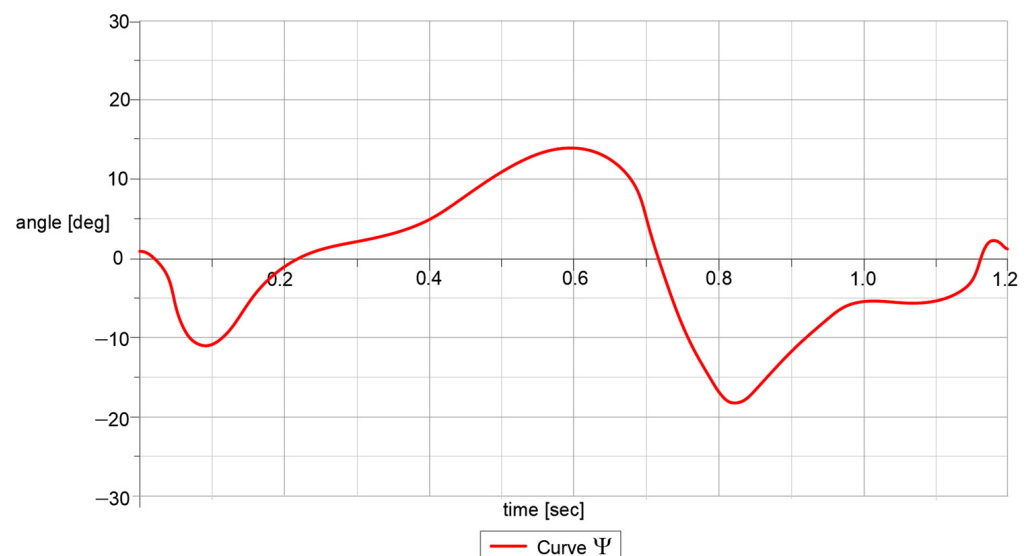


Figure 15. Computed ankle motion law represented by the angle ψ [degrees] for a complete gait cycle [seconds].

By having in sight these graphs reported in Figures 13–17, it can be observed that the obtained results are similar to the ones obtained throughout experimental tests, with a human participant. In addition the computational algorithm cannot be used in terms of a complete gait as 100%, and for this, the time function was chosen, which for a complete gait, the child used in experimental tests performs in 1.2 s. In the case of M point trajectory, this was computed from two components, namely x -axis component and y -axis component, as a function of time. After this, the numerical results were extracted and combined in another graph, i.e., the one in Figure 16.

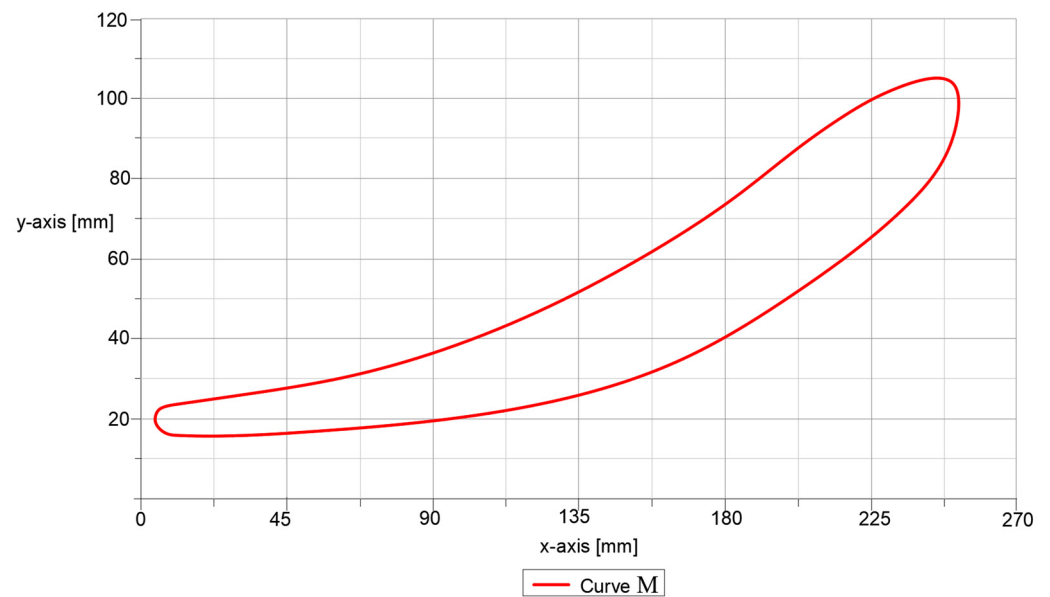


Figure 16. Computed trajectory of M-point [millimeters] for a complete gait cycle.

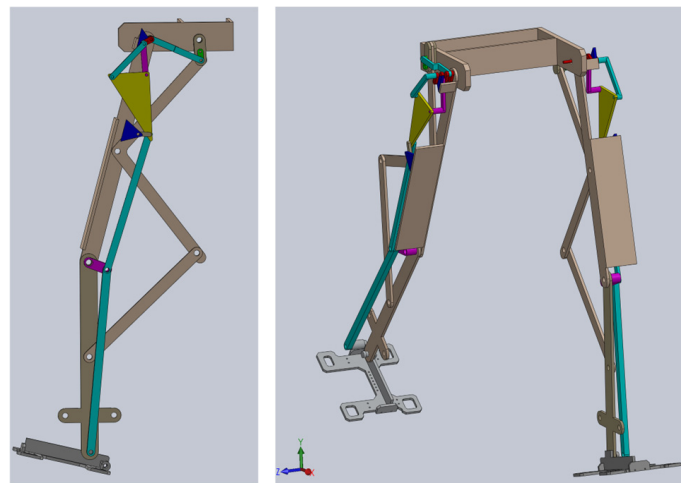


Figure 17. The CAD design of the proposed exoskeleton for numerical simulations.

5. CAD Design and Numerical Simulations

5.1. Lower Limb Exoskeleton Virtual Simulations

By having in sight the structural and kinematic schemes in Figures 9 and 10, and considering the dimensions used during numerical processing, a CAD model was created in a simplified parametrized form with the aid of SolidWorks software 2016. This lower limb exoskeleton model is shown in Figure 17, and it was created in a mirror position in order to have both legs. The aim of designing this was to better characterize the results from the kinematic analysis developed in the previous section.

An interface was created for exporting the CAD model, under the extension of a Para-solid file, to MSC ADAMS/Adams View software version R17 module. During virtual simulations, foot–ground contact was neglected. Also, the virtual model setup under the Adams View interface was made in accordance with data from [24].

The whole linkage was considered as made from aluminum alloy type 1060, with the following main characteristics: Elastic modulus— $69,000 \text{ N/mm}^2$, Poisson ratio—0.33, Mass density: 2700 kg/m^3 , Tensile strength: 68.9356 N/mm^2 .

There were defined 59 revolute joints, by taking into account the friction with the following data: static coefficient—0.01, dynamic coefficient—0.0025, pin radius of the ball joints—0.95 mm, stiction transition velocity—0.1, maximum stiction deformation—0.01.

Figure 18 shows the imported exoskeleton model under MSC Adams environment, where the defined revolute joints and links identification can be seen.

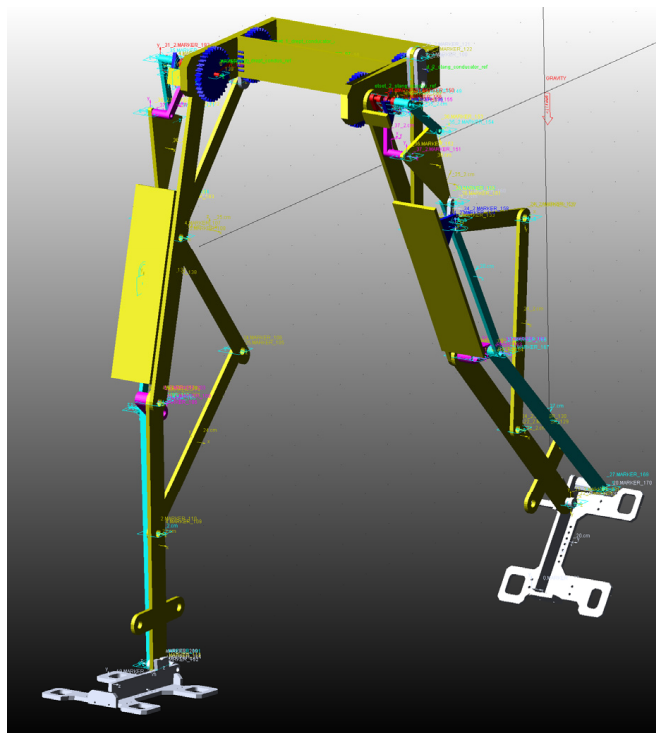


Figure 18. The designed exoskeleton linkage was imported in MSC Adams.

For simulations, initial conditions were considered like the ones for the child used in the experimental analysis frame. Thus, the exoskeleton linkage was placed in a biped position when the left lower limb start the gait phases, and the right one finished the gait phases, and these were in a close-loop action. The time period used in simulations was also defined and this was equal to 1.2 s, which corresponds to a complete gait.

A proper actuator was defined under the drive link no. 1 (which corresponds to Chebyshev and pantograph mechanism), and for actuating the Stephenson III six-bar mechanism it was defined as a pair of gears with a 1:1 ratio.

The actuator will rotate under a motion function depending on time and angular displacement ($30 \text{ degrees} \cdot \text{time}$), and the gears, there were considered the following parameters: gear width—8 mm; teeth number—33; axis center—85 mm; tooth angle—15 degrees; material—steel.

For the simulations, a GSTIFF solver with a defined error of 0.001 was used.

Thus, Figure 19 shows snapshots during a complete gait, and the snapshots were characterized by M-point trace and generating the specific trajectory.

Simulations were processed in order to determine the feasibility of the lower limb exoskeleton design and to characterize its operation features. Thus, the obtained results were represented by motion laws for the left hip, knee, and ankle joints. Obviously, the M point trajectory data were also obtained. These results were obtained in a numerical form, in order to perform a comparative motion analysis, as discussed in the next section.

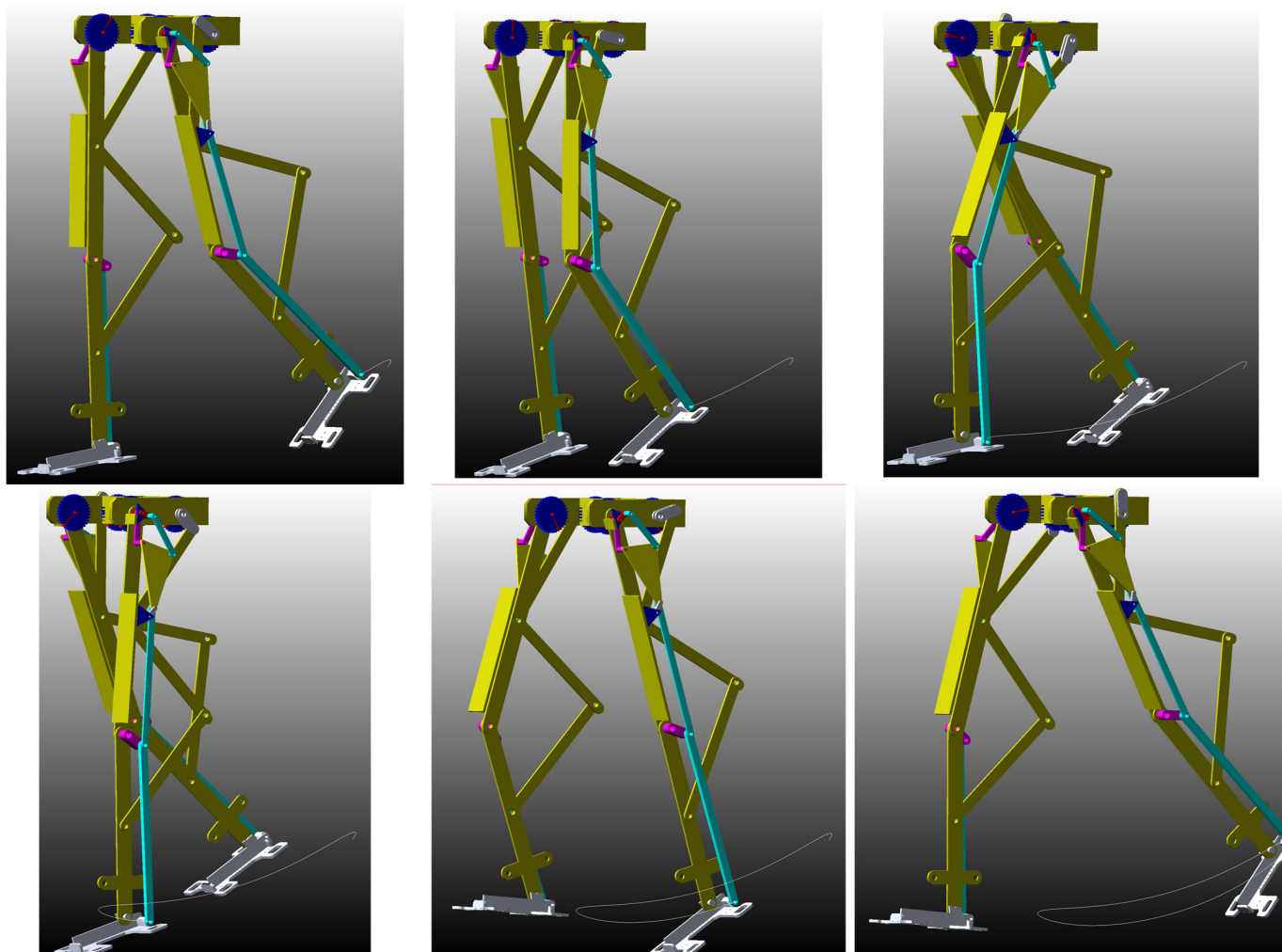


Figure 19. Snapshots during simulations of the proposed exoskeleton simplified model.

5.2. Results and Discussions

A comparative analysis was performed by using the numerical values of the obtained result, from experimental tests, kinematic model processing, and simulations under MSC Adams version R17 software.

For this, a specific import interface under LS-Dyna software version R12 was used in order to calculate the accuracy of the obtained results. At the beginning, for the input data, correspondence between notations was made. Thus, M4—point corresponds to the hip joint rotation center, namely $\gamma_{\text{hip}} = \varphi_3$; M21—point corresponds to the knee joint rotation center, respectively $\gamma_{\text{knee}} = \varphi_5$; M57—point corresponds to the ankle joint rotation center, namely $\gamma_{\text{ankle}} = \psi$. In the case of the foot trajectory, the correspondence was M67—point is M6—point from experimental analysis section and M—point from kinematic analysis section.

The input values were also filtered by using FFT filtering algorithm. In this way, results were obtained as the four plots reported in graphs in Figures 20–23.

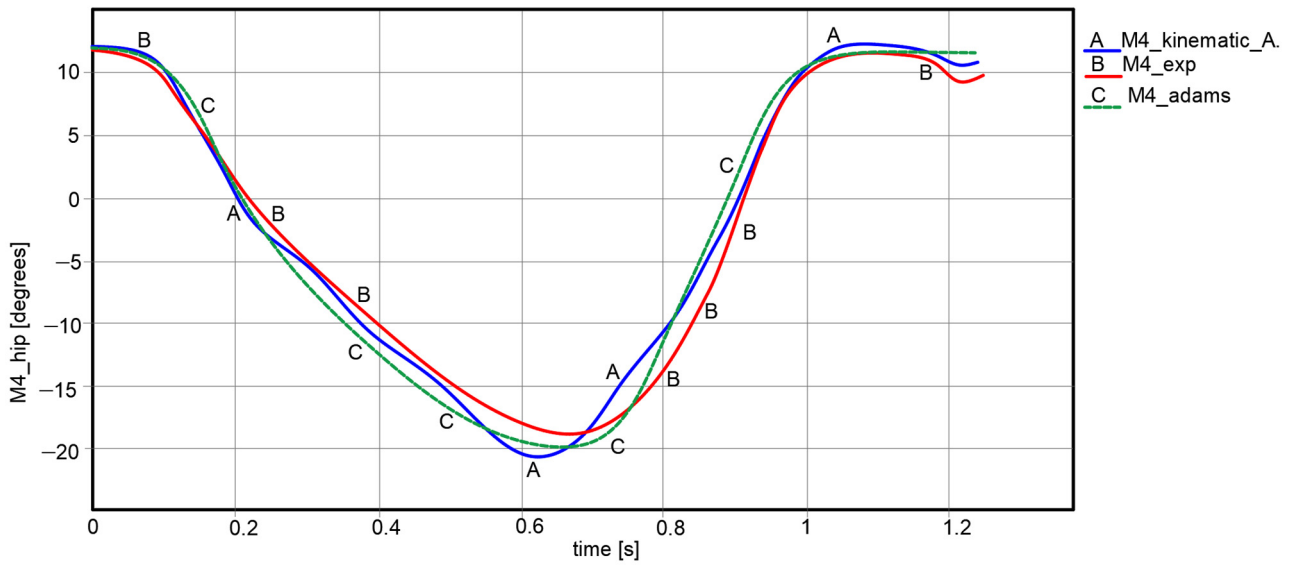


Figure 20. Comparison of analysis results for hip motion law [degrees] for a complete gait: A—kinematic analysis, B—experimental analysis, C—Adams simulation.

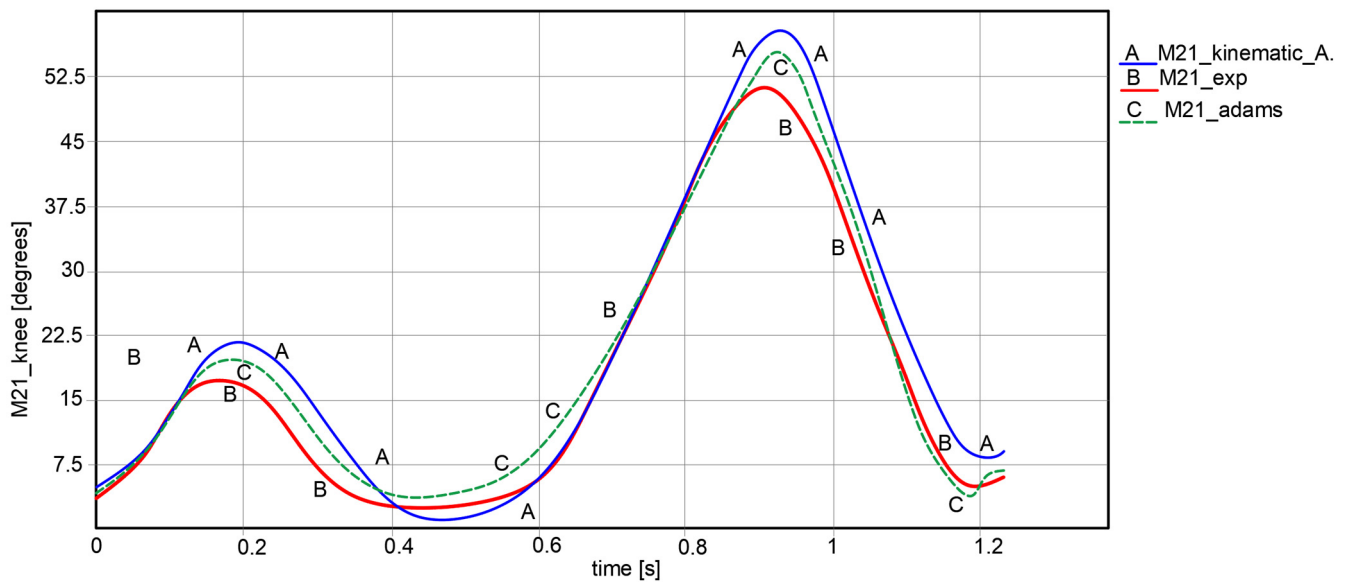


Figure 21. Comparison of analysis results for knee motion law [degrees] for a complete gait: A—kinematic analysis, B—experimental analysis, C—Adams simulation.

Using these diagrams, and with the aid of Ls-Dyna software version R12 module, maximum and minimum values were extracted, which are summarized in Table 2. Another reason for calling LS-Dyna module is that this program can estimate data accuracy for each obtained graph. The established accuracy is also indicated in Table 2.

An important note for the plots reported in Figures 20–23 is the one that the paths were appropriate one to another for all cases, respectively, experimental tests, kinematic analysis, and simulations with Adams software version R17.

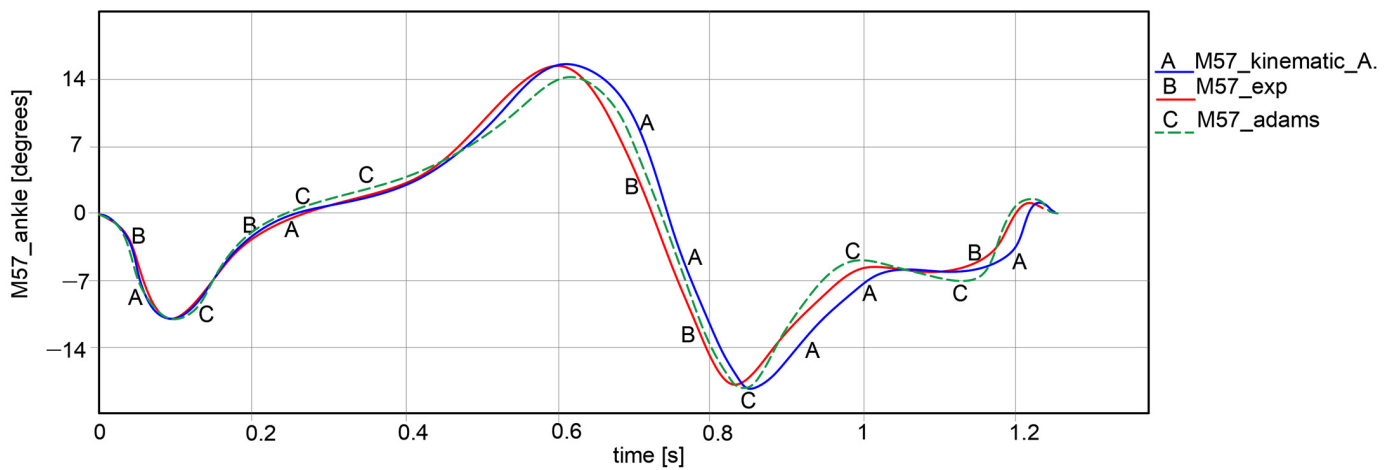


Figure 22. Comparative results for ankle motion law [degrees] for a complete gait: A—kinematic analysis, B—experimental analysis, C—Adams simulation.

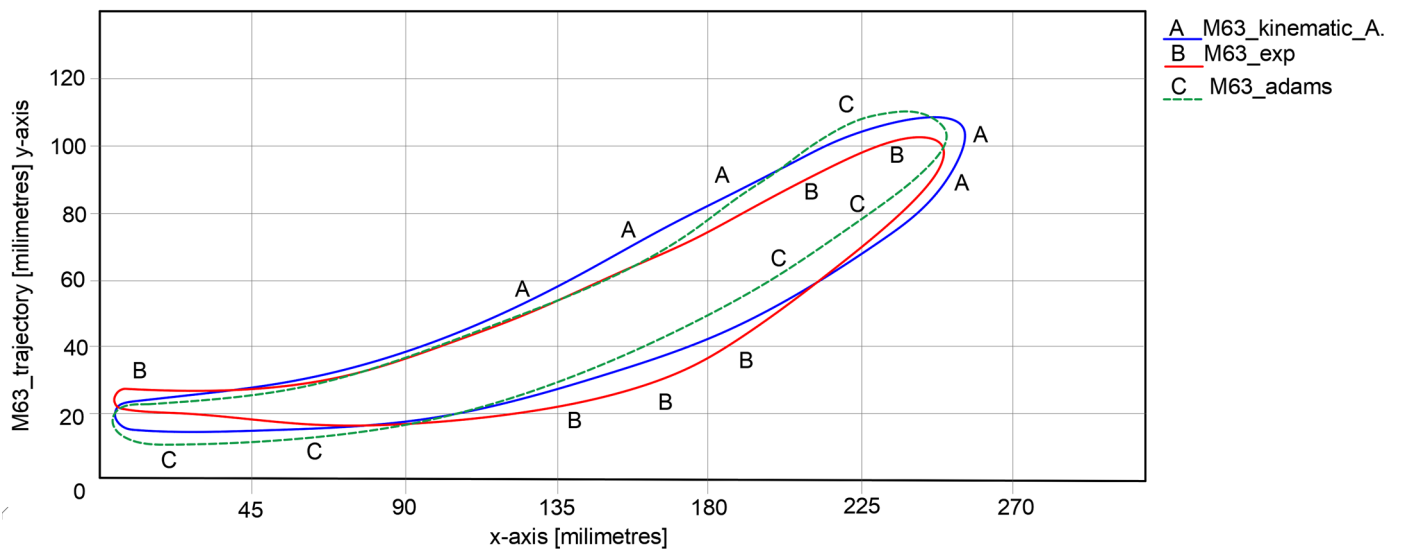


Figure 23. Comparative results for foot trajectory [millimeters] for a complete gait: A—kinematic analysis, B—experimental analysis, C—Adams simulation.

Table 2. Summary of comparison of results in the graphs from Figures 20–23.

Item	Experimental Analysis	Kinematic Analysis	Virtual Simulations	Accuracy
Hip joint	Max = 16.032 deg	Max = 17.887 deg	Max = 14.228 deg	2.32%
	Min = -18.557 deg	Min = -23.525 deg	Min = -20.032 deg	
Knee joint	Max = 50.088 deg	Max = 58.227 deg	Max = 54.064 deg	4.48%
	Min = 5.863 deg	Min = 3.573 deg	Min = 6.021 deg	
Ankle joint	Max = 14.773 deg	Max = 14.93 deg	Max = 14.022 deg	1.61%
	Min = -16.149 deg	Min = -18.771 deg	Min = -17.227 deg	
M point	yMax = 100.012 mm	yMax = 105.022 mm	yMax = 104.221 mm	3.96%
	yMin = 25.063 mm	yMin = 18.545 mm	yMin = 16.778 mm	
	xMax = 253.331 mm	xMax = 254.991 mm	xMax = 254.011 mm	2.05%
	xMin = 4.587 mm	xMin = 5.158 mm	xMin = 3.833 mm	

By having in sight the reported numerical values extracted from LS-Dyna, it can be remarked that the maximum numerical value of less accuracy reached a value of 4.48% in

the case of knee joint motion law. High accuracy was obtained in the case of ankle joints, respectively, a minimum numerical value of 1.61%. This represents that the Stephenson III six-bar mechanism had good behavior in a combined solution with the other two mechanisms. The whole lower limb exoskeleton average accuracy was 2.884%, and this value was under 5%, which represents the maximum accuracy value for validating the lower limb exoskeleton solution.

6. Conclusions

In this paper, a new design solution was proposed for a lower exoskeleton that has in its own structure two main mechanisms, namely a Chebyshev with a pantograph one and a modified Stephenson II six-bar mechanism. The presented solution had a complex structure but it can fulfill the criteria of low-cost and easy operation features due to the fact that is actuated with a single motor. Moreover, the proposed design represents a continuity of previous mechanisms being designed. The novelty of this mechanism is represented by the combination of the mentioned mechanisms that can actuate also motion at the ankle joint level. The proposed exoskeleton design has been characterized through numerical simulations with engineering software like Adams software version R17, with suitable models which respond to the design-specific purposes. The obtained results outline the exoskeleton operation and this validates the proposed solution in order to develop a prototype for gait assistance of the human user.

Author Contributions: Conceptualization, C.C. and M.C.; methodology, C.C. and M.C.; software, I.G.; validation, C.C., M.C. and A.M.; formal analysis, I.G.; investigation, C.C.; resources, D.P.; data curation, S.D. and I.G.; writing—original draft preparation, C.C.; writing—review and editing, C.C. and M.C.; visualization, D.P.; supervision, C.C. and M.C.; project administration, C.C.; funding acquisition, D.P. All authors have read and agreed to the published version of the manuscript.

Funding: This work was supported by a grant of the Ministry of Research, Innovation and Digitization, CCCDI—UEFISCDI, project number PN-III-P2-2.1-PED-2021-1917, within PNCDI III.

Data Availability Statement: Not applicable.

Conflicts of Interest: The authors declare no conflict of interest.

References

1. Carbone, G.; Ceccarelli, M. Legged robotic systems. In *Cutting Edge Robotics*; ARS Scientific Book: Wien, Austria, 2005; pp. 553–576.
2. Hirai, K.; Hirose, M.; Haikawa, Y.; Takenaka, T. The Development of Honda Humanoid Robot. In Proceedings of the IEEE International Conference Robotics and Automation, Leuven, Belgium, 16–20 May 1998; pp. 1321–1326.
3. Huang, G.T. Wearable Robots. *Technol. Rev.* **2004**, *4*, 70–73.
4. Li, T.; Ceccarelli, M. Design and simulated characteristics of a new biped mechanism. *Robotica* **2015**, *33*, 1568–1588. [[CrossRef](#)]
5. Shepherd, M.; Rouse, E. Design and validation of a Torque-Controllable knee exoskeleton for sit-to-stand assistance. *IEEE/ASME Trans. Mechatron.* **2017**, *22*, 1695–1704. [[CrossRef](#)]
6. Walsh, C.J.; Pasch, K.; Herr, H. An Autonomous, Under-Actuated Exoskeleton for Load-Carrying Augmentation. In Proceedings of the IEEE/RSJ International Conference on Intelligent Robots and Systems, (IROS), Beijing, China, 9–15 October 2006; pp. 1410–1415.
7. Walsh, C.J.; Paluska, D.; Pasch, K.; Grand, W.; Valiente, A.; Herr, H. Development of a Lightweight, Underactuated Exoskeleton for Load-Carrying Augmentation. In Proceedings of the IEEE International Conference on Robotics and Automation, Orlando, FL, USA, 15–19 May 2006; pp. 3485–3491.
8. Lerner, Z.; Damiano, D.; Bulea, T. A lower-extremity exoskeleton improves knee extension in children with crouch gait from cerebral palsy. *Sci. Transl. Med.* **2017**, *9*, eaam9145. [[CrossRef](#)] [[PubMed](#)]
9. Ganguly, A.; Sanz-Merodio, D.; Puyuelo, G. Wearable pediatric gait exoskeleton—A feasibility study. In Proceedings of the IEEE/RSJ International Conference on Intelligent Robots and Systems (IROS), Madrid, Spain, 1–5 October 2018; pp. 4667–4672.
10. Shieh, W.B.; Tsai, L.W.; Azarm, S. Design and optimization of a one-degree-of-freedom six-bar leg mechanism for a walking machine. *J. Robot. Syst.* **1997**, *14*, 871–880. [[CrossRef](#)]
11. Hesse, S.; Uhlenbrock, D.; Werner, C.; Bardeleben, A. A mechanized gait trainer for restoring gait in nonambulatory subjects. *Arch. Phys. Med. Rehabil.* **2000**, *81*, 1158–1161. [[CrossRef](#)] [[PubMed](#)]
12. Tsuge, B.; Plecnik, M.; McCarthy, J. Homotopy directed optimization to design a six-bar linkage for a lower limb with a natural ankle trajectory. *J. Mech. Robot.* **2016**, *8*, 061009. [[CrossRef](#)]

13. Wang, F.; Yu, C.; Tai-Yu, C.; Nai-Chun, C. Design and control of an active gait trainer. In Proceedings of the IEEE International Symposium on Industrial Electronics, Seoul, Republic of Korea, 5–8 July 2009.
14. Shao, Y.; Xiang, Z.; Liu, H.; Li, L. Conceptual design and dimensional synthesis of cam-linkage mechanisms for gait rehabilitation. *Mech. Mach. Theory* **2016**, *104*, 31–42. [[CrossRef](#)]
15. Sabaapour, M.R.; Lee, H.; Afzal, M.R.; Eizad, A.; Yoon, J. Development of a Novel Gait Rehabilitation Device with Hip Interaction and a Single DOF Mechanism. In Proceedings of the 2019 International Conference on Robotics and Automation, ICRA, Montreal, QC, Canada, 20–24 May 2019.
16. Haghjoo, M.R.; Lee, H.; Afzal, M.R.; Eizad, A.; Yoon, J. Mech-Walker: A novel single-DOF linkage device with movable frame for gait rehabilitation. *IEEE/ASME Trans. Mechatron.* **2021**, *26*, 13–23. [[CrossRef](#)]
17. Tsuge, B.Y.; McCarthy, J.M. *Synthesis of a 10-Bar Linkage to Guide the Gait Cycle of the Human Leg*; ASME: Boston, MA, USA, 2015.
18. Copilusi, C.; Ceccarelli, M.; Dumitru, N.; Carbone, G. Design and Simulation of a Leg Exoskeleton Linkage for a Human Rehabilitation System. In *The 11th IFToMM International Symposium on Science of Mechanisms and Machines. Mechanisms and Machine Science*; Springer: Cham, Switzerland, 2016; Volume 18.
19. Kapsalyamov, A.; Hussain, S.; Brown, N.A.; Goecke, R.; Hayat, M.; Jamwal, P.K. Synthesis of a six-bar mechanism for generating knee and ankle motion trajectories using deep generative neural network. *Eng. Appl. Artif. Intell.* **2023**, *117*, 105500. [[CrossRef](#)]
20. Plecnik, M.; McCarthy, J.M. Design of Stephenson linkages that guide a point along a specified trajectory. *Mech. Mach. Theory* **2016**, *96 Pt 1*, 38–51. [[CrossRef](#)]
21. CONTEMPLAS Motion Analysis Equipment User Manual. 2010.
22. Williams, M. *Biomechanics of Human Motion*; Saunders Co.: Philadelphia, PA, USA; London, UK, 1996.
23. Copilusi, C.; Ceccarelli, M.; Dumitru, S.; Margine, A.; Geonea, I. A Leg Exoskeleton Mechanism for Human Walking Assistance. In *New Trends in Medical and Service Robotics. MESROB 2023. Mechanisms and Machine Science*; Springer: Cham, Switzerland, 2023; Volume 133.
24. MSC Adams Software User Manual. 2010.

Disclaimer/Publisher’s Note: The statements, opinions and data contained in all publications are solely those of the individual author(s) and contributor(s) and not of MDPI and/or the editor(s). MDPI and/or the editor(s) disclaim responsibility for any injury to people or property resulting from any ideas, methods, instructions or products referred to in the content.